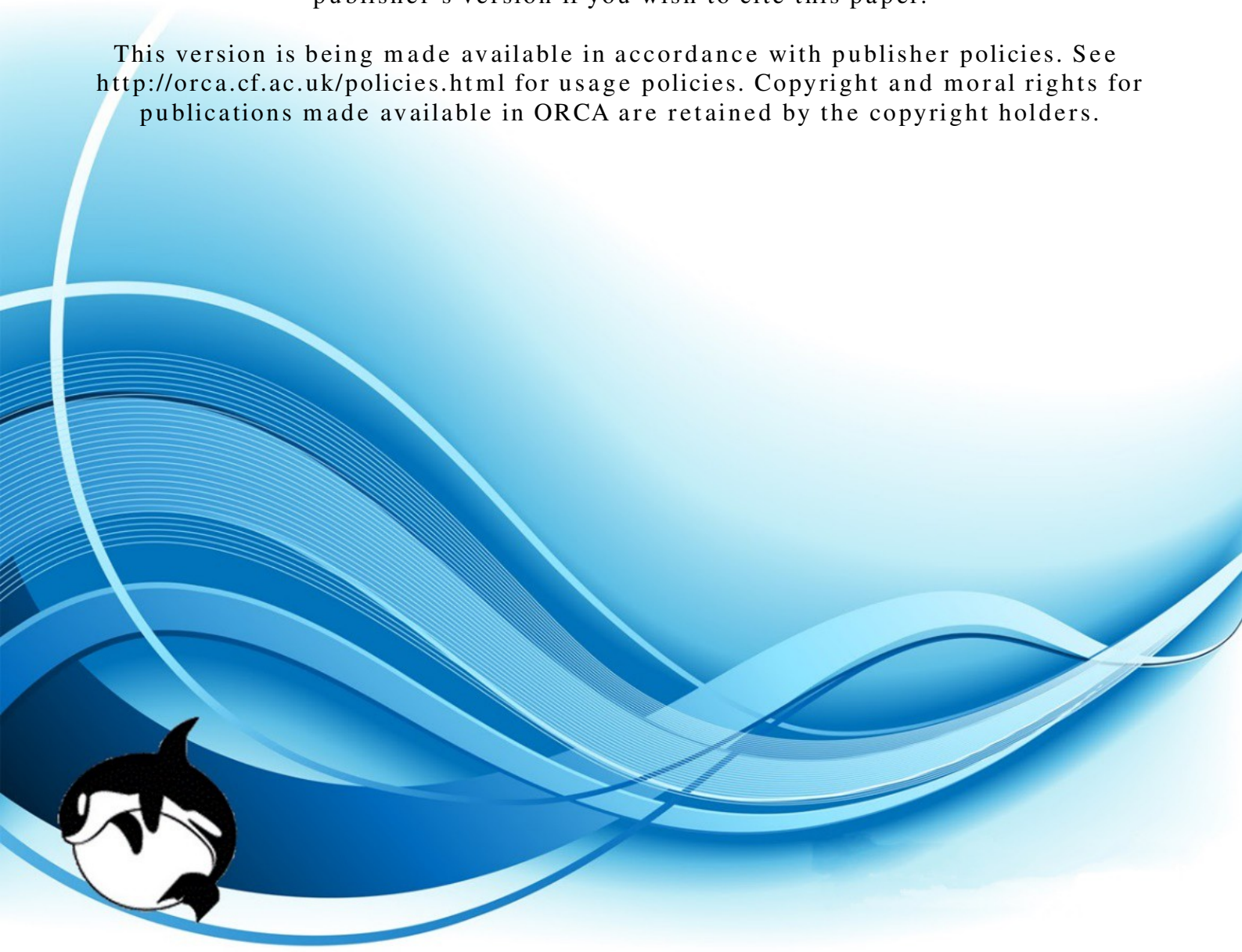

COLOURED NOISE FROM STOCHASTIC INFLOWS IN REACTION-DIFFUSION SYSTEMS

MICHAEL F ADAMER *, HEATHER A HARRINGTON †, EAMONN A GAFFNEY‡, AND THOMAS E WOOLLEY§

Abstract. In this paper we present a framework for investigating coloured noise in reaction-diffusion systems. We start by considering a deterministic reaction-diffusion equation and show how external forcing can cause temporally correlated or coloured noise. Here, the main source of external noise is considered to be fluctuations in the parameter values representing the inflow of particles to the system. First, we determine which reaction systems, driven by extrinsic noise, can admit only one steady state, so that effects, such as stochastic switching, are precluded from our analysis. To analyse the steady state behaviour of reaction systems, even if the parameter values are changing, necessitates a parameter-free approach, which has been central to algebraic analysis in chemical reaction network theory. To identify suitable models we use tools from real algebraic geometry that link the network structure to its dynamical properties. We then make a connection to internal noise models and show how power spectral methods can be used to predict stochastically driven patterns in systems with coloured noise. In simple cases we show that the power spectrum of the coloured noise process and the power spectrum of the reaction-diffusion system modelled with white noise multiply to give the power spectrum of the coloured noise reaction-diffusion system.

1. Introduction. One of the central challenges in mathematical biology is understanding mechanisms involved in development processes. Within the context of developmental biology, the emergence of large scale spatial structure, has often been theoretically explored through a common framework of deterministic partial differential equations defining reaction-diffusion systems [1, 2, 3]. While current frameworks may explain a variety of phenomena in development, they can also suffer from over-simplification [4], with the additional caveat that finding theoretical models both consistent with mechanism-based knowledge and capable of predicting observed patterns is a highly complex task, suffering from both model and parameter fine tuning [5, 6].

Many models that describe pattern formation assume parameters are constant; however, this deterministic assumption is not suitable for certain conditions. Some systems are better suited towards a stochastic approach. When a system is coupled to external and stochastic drivers, then the parameter values can change. The stochastic driving is often represented by stochastic parameters, that is a parameter which is drawn from a certain distribution at each time step or spatial point, and referred to as *extrinsic noise* below. This contrasts with most previous work on stochastic pattern formation, referred to as *intrinsic noise*, which assumes low copy number and it does not assume external drivers as the source of noise [7, 8, 4, 9, 10, 11]. Extrinsic noise has been studied extensively in [12], however, not in the context of chemical reaction network theory and reaction-diffusion systems.

The structure of intrinsic noise is often taken to be be highly constrained and in particular uncorrelated in time, leading to white noise representations. For instance, if the noise is due to low copy number induced dynamics, Gaussian white noise forcing emerges from the chemical Langevin equation approximation to the chemical master equation [13]. Even with such constraints there is a rich diversity of noise-induced

*Wolfson Centre for Mathematical Biology, Mathematical Institute, University of Oxford (adamer@maths.ox.ac.uk).

†Wolfson Centre for Mathematical Biology, Mathematical Institute, University of Oxford.

‡Wolfson Centre for Mathematical Biology, Mathematical Institute, University of Oxford.

§Cardiff School of Mathematics, Cardiff University.

phenomena, such as spatio-temporal pattern formation [7, 10], stochastic oscillations [8], metastability [4], waves [9] or enhanced oscillation amplitude [14] and a general introduction to the effects of noise in spatial system can be found in [15].

However, when the source of the noise is *extrinsic*, other forms of noise are permissible. In particular, the defining special properties of white noise may in general be relaxed and hence stochastic forcing can emerge with non-trivial temporal correlations, often termed *coloured noise*. Our objective is to show how extrinsic noise influences spatio-temporal reaction-diffusion patterns, in particular by developing power spectral methods to analyse the impact of coloured noise. In this paper it is assumed that the effects of intrinsic noise are negligible and only the extrinsic noise provides a stochastic perturbation of the system. Therefore, in contrast to internal noise models, the common description of a stochastic chemical reaction network as a continuous time Markov chain (and its computational solution via the Gillespie algorithm [16]) cannot typically be applied.

To proceed, we abstract the biological system to a chemical reaction network and use techniques from the mathematical modelling of chemical reaction networks. However, for biological interpretations it is imperative to remember that many cellular processes are governed by biochemical reactions [17] and, hence, can be described by chemical reaction networks. First, we note that deterministic pattern formation reaction diffusion systems in biological applications with n interacting biochemical species take the form [3, 1]

$$\frac{\partial \boldsymbol{x}}{\partial t} = \boldsymbol{D}\frac{\partial^2 \boldsymbol{x}}{\partial s^2} + \boldsymbol{f}(\boldsymbol{x}) \tag{1.1}$$

in one spatial dimension, where $\boldsymbol{x} \in \mathbb{R}^n_{\geq 0}$ is a vector of n chemical concentrations. The models we consider are networks with *mass action kinetics* [18], rendering the term $\boldsymbol{f}(\boldsymbol{x}) = (f_1(\boldsymbol{x}), \ldots, f_n(\boldsymbol{x}))^T$ a vector of polynomial functions. The polynomials describe the underlying reaction network between the species and $\boldsymbol{D}(\partial^2\boldsymbol{x}/\partial s^2)$ with $\boldsymbol{D} = \mathrm{diag}(D_1, \ldots, D_n)$ describes the diffusion of $\boldsymbol{x}$. Let there be M chemical reactions in the spatially homogeneous system whose dynamics are described by $\partial\boldsymbol{x}/\partial t = \boldsymbol{f}(\boldsymbol{x})$. Each reaction is parametrised by a reaction rate $k_i > 0$ and therefore we have a vector of reaction rates $\boldsymbol{k} = (k_1, \ldots, k_M) \in \mathbb{R}^M_{>0}$. Throughout this paper we use homogeneous Neumann boundary conditions

$$\left.\frac{\partial \boldsymbol{x}}{\partial s}\right|_{s=0,L} = 0\,, \tag{1.2}$$

where L is the domain length. Note that, although our work is only applied to systems of one spatial dimension, the theory can easily be extended to an arbitrary number of spatial dimensions.

Counter-intuitively, it has been shown that under certain conditions [1] diffusion can drive an otherwise spatially uniform stable state to instability. Such unstable systems, which can form stable patterns, such as stripes or spots, are called *Turing Systems* [3, 19]. To avoid the complications of bistable dynamics, and later stochastic analogues such as switching between steady states, we impose the constraint that the spatially homogeneous solution has a unique stable steady state, $\boldsymbol{x}^*$, such that $\boldsymbol{f}(\boldsymbol{x}^*) = 0$ [1]. To find models which have this property we use techniques from real algebraic geometry [20] which provides simple tools, which ensure there exists only a single steady state in a model. Since Turing's work in 1952 many biological patterning systems have been suggested to be Turing systems [21, 22, 23].

Fundamentally, the application of a set of partial differential equation (PDE) models for a biochemical reaction system assumes that the species of interest are in high enough concentration to allow continuum modelling. By contrast, when the number of particles in the biological system is low, intrinsic stochasticity of the system must be included in the model [7, 10, 8, 4, 9], which typically yields studies that investigate the impact of white noise.

However, as mentioned, stochasticity in biological systems can also arise from extrinsic noise and hence temporal variations in parameter values [24]. Thus, instead we generalise the deterministic system to include *stochastic* parameter values. Specifically, we focus on the effect of stochastic fluctuations in the constant term, the "inflow" term, of the chemical reaction network $\boldsymbol{f}(\boldsymbol{x})$. As the extrinsic noise can arise from a vast number of different mechanisms, such as varying experimental conditions [25], it is largely free of microscopic constraints, especially the absence of temporal correlation. However, the impact of correlated external noise has, to the authors' knowledge, received little theoretical modelling attention. Thus we proceed to develop a framework to study external coloured noise forcing of the above deterministic system for pattern formation in biologically motivated scenarios, analysing how temporal correlation in noise, as described by colour, impacts self-organisation properties.

The paper is organised as follows. In section 2 we introduce required notions of chemical reaction network theory to select a class of models relevant to our framework, i.e. those whose number of steady states is unaltered by changes in parameter values, temporal or otherwise. We then introduce stochastic inflow parameters and describe their connection coloured noise. In section 3 we highlight the impact of noise colouring on the spatio-temporal patterns formed by example of the Schnakenberg system. In particular, we discuss noise arising from stochastic subnetworks and varying experimental conditions. Our numerical results are discussed in section 4 where we summarise the distinguishable differences between the various noise colours.

2. Theoretical Background and Power Spectra Analysis. In this section we introduce the theoretical background of this paper.

2.1. Chemical Reaction Network Theory. A central aim of chemical reaction network theory (CRNT) is to describe the properties of a chemical reaction network from its reaction graph alone [26, 27]. One such property is the capacity for multiple steady states. Define a chemical reaction network by the multi-set $\mathcal{N} = \{\mathcal{S}, \mathcal{C}, \mathcal{R}\}$, where $\mathcal{S}, \mathcal{C}, \mathcal{R}$ are defined below. We begin by embedding the network into n dimensional Euclidean space $\mathbb{R}^n$ by associating a basis vector $\boldsymbol{e}_i$ to each chemical species X_i such that $X_1 \to \boldsymbol{e}_1 = (1, 0, 0, \dots)^T$, $X_2 \to \boldsymbol{e}_2 = (0, 1, 0, \dots)^T$ and so on. Let $\mathcal{S} = \{X_1, \dots, X_n\}$ be the set of all chemical species in the network, then a generic reaction can be expressed as

$$\sum_{i=1}^{n} \alpha_i X_i \xrightarrow{k} \sum_{i=1}^{n} \beta_i X_i \ . \tag{2.1}$$

The constants α_i and β_i are *stoichiometric coefficients* which give information about how many molecules of X_i are consumed and produced in each reaction. By letting $X_i \to \boldsymbol{e}_i$ we can formulate a *reaction vector* describing the consumption, or production, of a species X_i in a reaction

$$\boldsymbol{r} = \sum_{i=1}^{n} (\beta_i - \alpha_i)\boldsymbol{e}_i \ . \tag{2.2}$$

If an entry of $\boldsymbol{r}$ is negative, then a species is consumed, whilst if an entry of $\boldsymbol{r}$ is positive, then a species is produced.

Denote the set of all reaction vectors in a network by $\mathcal{R} = \{\boldsymbol{r}_1, \ldots, \boldsymbol{r}_M\}$. To complete the description of a chemical reaction network in terms of sets and their embedding into Euclidean space we introduce the notion of *complexes*. Complexes are linear combinations of species which appear on the left or right hand sides of reaction vectors. In equation (2.1) the two complexes are $C_1 = \sum_{i=1}^{n} \alpha_i X_i$ and $C_2 = \sum_{i=1}^{n} \beta_i X_i$, where C_1 is the *reactant complex* and C_2 is the *product complex*. Let the set of all complexes be $\mathcal{C} = \{C_1, \ldots, C_l\}$. The reaction network, $\mathcal{N}$, is therefore a directed graph with vertex set $\mathcal{C}$ and a directed edge between vertices C_i and C_j if and only if $C_j - C_i \in \mathcal{R}$, with the same embedding, $X_i \to \boldsymbol{e}_i$. Note that the description of the reaction network *does not* include any notion of rate constants k, however, many results in chemical reaction network theory include the reaction rates explicitly as a positive vector $\boldsymbol{k} = (k_1, \ldots, k_m)^T \in \mathbb{R}^M_{>0}$.

In this paper we study the influence of noise on reaction-diffusion systems that are able to produce patterns in a well-defined parameter region. Critically, we will see that coloured noise is able to have both a constructive influence outside of this previously defined parameter region (i.e. the noise stabilises patterns where we would not expect them deterministically), as well as a destructive influence on patterns which normally would arise. In particular, we would like to exclude the intrinsically stochastic effect of *stochastic switching*, which occurs for a system that has multiple steady states in some parameter region. Stochastic switching describes the phenomenon that a chemical reaction network can jump from one steady state to another when subject to finite stochastic perturbations. To avoid this scenario we use a network structure based tool described in [20] which a priori excludes multistationarity.

Take a chemical reaction network $\mathcal{N}$ and embed its complexes and reactions into $\mathbb{R}^n$. Then define the matrices $m_1 = (\boldsymbol{r}_1 \boldsymbol{r}_2 \cdots \boldsymbol{r}_M)$ for $r_i \in \mathcal{R}$ and $m_2^T = (\boldsymbol{b}_1 \boldsymbol{b}_2 \cdots \boldsymbol{b}_r)$ where $\{\boldsymbol{b}_i\}$ is the set of reactant complex vectors of $\mathcal{N}$. Let $diag(k_1, \ldots, k_M)$ be the diagonal matrix of reaction constants. Using the law of mass action the dynamics of the species concentrations can be described by

$$\frac{d\boldsymbol{x}}{dt} = \boldsymbol{f}(\boldsymbol{x}) = m_1 \, diag(k_1, \ldots, k_m) \, \boldsymbol{x}^{m_2} \tag{2.3}$$

where $\boldsymbol{x}^{m_2} = (x_1^{b_{11}} x_2^{b_{12}} \cdots x_n^{b_{1n}}, \ldots, x_1^{b_{M1}} x_2^{b_{M2}} \cdots x_n^{b_{Mn}})^T$. Note that the reactant complexes and the reactions are structural properties of the reaction graph. Further, let $\boldsymbol{a} \in \mathbb{R}^n$ and define its sign vector $\sigma(\boldsymbol{a}) = \{-, 0, +\}^n$ by applying the sign function to each component of $\boldsymbol{a}$. Therefore, the i^{th} component of the sign vector $\sigma(\boldsymbol{a})_i = \text{sign}(a_i) \in \{+, 0, -\}$.

The link from network structure to multistationarity is outlined in [20, Theorem 1.4] and it concerns the injectivity of the map $\boldsymbol{f} : \boldsymbol{x} \mapsto d\boldsymbol{x}/dt$. If $\boldsymbol{f}(\boldsymbol{x})$ is injective then there exists a unique vector $\boldsymbol{x}^* \in \mathbb{R}^n$ such that $\boldsymbol{f}(\boldsymbol{x}^*) = 0$. In other words the network is monostationary. The conditions for an injective $\boldsymbol{f}(\boldsymbol{x})$ hold for all parameter values $\boldsymbol{k} = (k_1, \ldots, k_M)$. A corollary of [20, Theorem 1.4] is that $\boldsymbol{f}(\boldsymbol{x})$ is injective if

$$\ker(m_2) = \{0\} \text{ and } \sigma(\ker(m_1)) \cap \sigma(\text{im}(m_2)) = \{0\} \, . \tag{2.4}$$

Note, that this condition depends on the network structure, specifically, the spaces spanned by the kernel of the reaction matrix, m_1, and the image of the source complex matrix, m_2, but not on the parameter values.

2.2. Stochastic Inflow in Chemical Reaction Networks. We will now show how chemical reaction networks (CRNs) that satisfy injectivity (preclusion of multistationarity) can be applied to consider parameter stochasticity, especially, to the case of stochastic inflows. In particular, this subsection serves to show the mathematical equivalence between stochastic inflows and internal noise systems but also to introduce a novel way of modelling external noise in chemical reaction networks. Readers interested in applying coloured noise to stochastic reaction-diffusion equations with internal noise modelled by reaction-diffusion PDEs or Chemical Langevin Equations may skip this subsection.

Much effort in the CRNT literature investigates the effect of inflows into the chemical system, especially when the network is changed to a "fully open system" in which every species has an inflow reaction [28, 29, 30, 31]. By contrast, here we change the nature of the model by generalising the inflow reaction rates to stochastic processes, rather than simply adding inflow processes as deterministic reactions. It should be noted that despite the name we do not assume that these reactions are inflows into the domain of simulation, rather, the inflow reactions correspond to the creation of particles from some other process which happens *throughout the domain*. Sometimes these inflow reactions are the called"inputs" in engineering applications and the concentrations are the "outputs" and, therefore the study of chemical reaction networks with varying inflows can be rephrased into a study of the "input-output" relation as has been the approach in previous work [32].

Consider a chemical reaction network $\mathcal{N}$. An *inflow* reaction for species X_i is manifested in the reaction graph as

$$\emptyset \xrightarrow{k_{\text{in}}} X_i \ .$$

Usually, the work in CRNT assumes the reaction rate k_{in} to be constant in time (and space). However, the zero complex, $\emptyset$, symbolises a process not included in the model such as the the production of X_i by another network, which we call an "auxiliary network", or a mechanical addition of X_i to an experimental setup. Both mechanisms are often subsumed into $\emptyset$ and usually approximated as constant or "perfect" inflow, however, they can exhibit intricate dynamics. We model the dynamics of "non-perfect" inflows by a stochastic process whose origin can be two-fold.

(a) *Stochastic sub-systems*: We assume that the inflow into the (deterministic) reaction diffusion system is provided by the output of another chemical reaction network (with a unique fixed point). When the number of particles in the *auxiliary network* is large the system will be in a steady state and the inflow rate k_{in} will simply be proportional to the steady state value of a species of the auxiliary system. However, when the particle number in the auxiliary system is low, stochastic fluctuations cannot be ignored and, while still proportional to the concentration of a species in the subsystem, the actual influx parameter k_{in} will be a stochastic process $K_{\text{in}}(t)$. Due to correlations and interactions within the auxiliary system $K_{\text{in}}(t)$ may not simply be white noise.

(b) *Experimental fluctuations*: In chemical engineering it is assumed that inflow of chemicals into a reactor is a perfectly deterministic process, however, due to mechanical or other experimental imperfections the inflow into a reaction can vary stochastically. This again renders the influx parameter k_{in} into a stochastic process $K_{\text{in}}(t)$.

Whereas the two sources of parameter noise are conceptually different, their math-

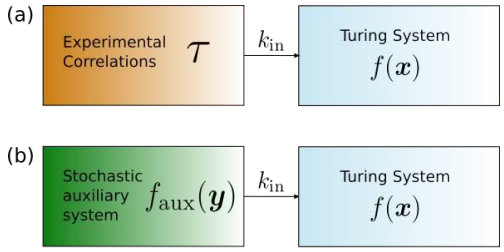

Fig. 1: The two mechanisms contributing to stochastic inflows. The boxes on the left are usually treated as black boxes resulting in some constant inflow modelled by the parameter k_{in}. We differentiate between experimental fluctuations, symbolised by a correlation τ in (a) and auxiliary networks described by $f_{\text{aux}}(\boldsymbol{y})$ in case (b).

ematical description is the same. Consider a stochastic process $K(t)$ with an underlying distribution $\mathcal{D}(t)$. Therefore, at every time t we have $K(t) \sim \mathcal{D}(t)$. To be biologically relevant (i.e. to ensure all chemical concentrations are non-negative at every t) we require $\mathcal{D} = 0$ for all $K(t) < 0$ and, hence, the distribution $\mathcal{D}$ needs to be continuous almost everywhere. To simplify the following mathematical analysis we approximate the distribution of $K(t)$ as a *truncated Gaussian*, since we would like to connect our analysis to the internal noise case. Future work could focus on other non-negative distributions, such as the log-normal distribution, on a continuous probability space. Therefore, we can describe $K(t)$ as

$$\begin{aligned} K(0) &= k, \\ \Delta K &= K(t) - \mathbb{E}\left[K(t')\right] = \frac{1}{\sqrt{\Omega}}\sqrt{g(t,t')}\xi, \\ K(t) &= 0 \qquad \text{if } \Delta K < -\mathbb{E}\left[K(t')\right], \end{aligned}$$

such that:

$$\mathbb{E}[K(t)] = k \quad \forall t \geq 0, \tag{2.5}$$

where $\xi \sim N(0,1)$, Ω is positive constant and $g(t,t')$ is a positive function. We assume that the standard deviation of the Gaussian perturbation to the mean parameter value is small such that $K(t) < 0$ is a rare event. Due to the negligible truncation, we approximate the moments of the truncated Gaussian as the moments of the full Gaussian such that $\langle K(t) - k\rangle = 0$ and $\langle (K(t)-k)(K(t')-k)\rangle = \Omega^{-1} g(t,t')$. In other words, the small exponential tail which is truncated would only provide a negligible perturbation to the moments of the non-truncated Gaussian. The validity of this assumption is confirmed in the computational results of Section 3. In the remainder of this paper we will show how various functions $g(t,t')$ can arise in mathematical modelling, especially when stochastic auxiliary networks are considered.

We can further connect the parameter Ω to physical quantities of the underlying chemical reaction network by again considering the sources of stochastic inflow. We assume that the origin of the stochastic inflow is stochastic auxiliary networks or experimental imperfections. Therefore, in the limit of either a perfect experiment or a deterministic auxiliary network the inflow should be deterministic and

$\langle (K(t)-k)(K(t')-k)\rangle = 0$ implying $\Omega \to \infty$. For stochastic auxiliary networks the quantity Ω which parametrises the size of the stochastic fluctuations can be related to the *system size* [33]. Similarly to the system size expansion, we require Ω to be sufficiently large. Large Ω helps to maintain a positive solution of the stochastic partial differential equation, although, positivity cannot be guaranteed when the noise is correlated suggesting a breakdown of the modelling assumptions for such events.

Next, consider a chemical reaction network $\mathcal{N}$ in which a subset of species has an inflow reaction. Denote the set of species with (stochastic) inflow by $\mathcal{S}_{\text{in}} \subseteq \mathcal{S}$. If there is more than one (stochastic) inflow $|\mathcal{S}_{\text{in}}| > 1$ the stochastic process will be a multi-dimensional version of (2.5). Further, assume that the stochastic process has a spatial dependence. The description of the stochastic process outlined in this section still applies in this case, if we have $\boldsymbol{K}_{\text{in}}(t,s)$ as the vector of stochastic inflow such that

$$\mathbb{E}[\boldsymbol{K}_{\text{in}}(t,s)] = \boldsymbol{k}_{\text{in}}$$

and

$$\boldsymbol{K}_{\text{in}}(t,s) - \mathbb{E}\left[\boldsymbol{K}_{\text{in}}(t',s)\right] = \boldsymbol{\eta}(s)$$

with

$$\begin{aligned} \langle \boldsymbol{\eta} \rangle &= 0 \\ \langle \boldsymbol{\eta}\boldsymbol{\eta}^T \rangle &= B(s,s')G(t,t') \\ &= \{B_{ij}(s,s')G_{ij}(t,t')\} \end{aligned} \tag{2.6}$$

and $B(s,s')$ representing the potential covariances between the stochastic inflows.

Since our assumptions made the inflow process additive and uncoupled to the species, the stochastic reaction network can be described by the system of stochastic partial differential equations (SPDEs)

$$\frac{\partial \boldsymbol{x}}{\partial t} = D\frac{\partial^2 \boldsymbol{x}}{\partial s^2} + \boldsymbol{f}(\boldsymbol{x}) + \frac{1}{\sqrt{\Omega}}\boldsymbol{\eta}\,, \tag{2.7}$$

where $\boldsymbol{\eta}$ is a vector of stochastic processes such that its support is $supp(\boldsymbol{\eta}) = \mathcal{S}_{\text{in}}$.

Note that in our limit randomising inflows leaves $\mathcal{N}$ as well as $\boldsymbol{f}(\boldsymbol{x})$ invariant, and hence, the steady state structure of the system; i.e. if we start out with an injective function $\boldsymbol{f}(\boldsymbol{x})$ then adding stochasticity will not change this injectivity.

The assumption of rate constants being stochastic processes rather than constants can be extended to non-inflow reactions too. However, equation (2.7) will have extra terms of multiplicative noise. In the next section we study perturbations to the steady state whose scaling will render the study of non-inflow stochastic reaction rates a trivial extension of the analysis of this subsection.

Further, it should be added that in this paper it is assumed that in the system under study internal noise is negligible compared to the effects of external noise. However, if internal noise was to be included, then the inflow rate constants could be modified in a chemical master equation which could be simplified using a weak noise expansion. Care needs to be taken, however, when judging system sizes as the external system size, here denoted as Ω, may be considerably different from the internal system size.

2.3. Power Spectra for Stochastic Inflows. To fully classify the patterns arising from the addition of stochastic inflows we calculate the power spectra of the patterns. Power spectra are an analytic tool showing which spatial and temporal frequencies are present in a pattern [34, 7, 35]. Peaks in power spectra give information about dominant frequencies and, hence, about oscillatory behaviour of a system in space and time.

First, we linearise equation (2.7) about the fixed point $\boldsymbol{x} \sim \boldsymbol{x}^* + \overline{\delta \boldsymbol{x}}$, where $\overline{\delta \boldsymbol{x}}$ represent small perturbations. These perturbations should decay in the deterministic limit as the system will converge to the steady state outside the Turing parameter regime. Inside the Turing regime the system is assumed to converge to a stable pattern rather than a stable state which is not considered in this paper. Hence, our analysis is valid only *outside* the Turing pattern regime. Substituting the linearisation ansatz into equation (2.7) and keeping lowest order terms only we get

$$\frac{\partial \overline{\delta \boldsymbol{x}}}{\partial t} = D \frac{\partial^2 \overline{\delta \boldsymbol{x}}}{\partial s^2} + J|_{\boldsymbol{x}=\boldsymbol{x}^*} \overline{\delta \boldsymbol{x}} + \frac{1}{\sqrt{\Omega}} \boldsymbol{\eta} \,, \tag{2.8}$$

where $J|_{\boldsymbol{x}=\boldsymbol{x}^*}$ is the Jacobian of $\boldsymbol{f}(\boldsymbol{x})$ evaluated at the fixed point $\boldsymbol{x}^*$, which for notational convenience we will denote as J.

We make one further assumption, namely the scaling of the perturbation $\overline{\delta \boldsymbol{x}}$ with the parameter Ω controlling the magnitude of the stochastic input. Let $\overline{\delta \boldsymbol{x}} = \Omega^\alpha \delta \boldsymbol{x}$. Then, if $\alpha < -1/2$ and in the limit of $\Omega \to \infty$ the leading order term is the stochastic process $\boldsymbol{\eta}$ only, similarly, if $\alpha > -1/2$, then $\boldsymbol{\eta}$ could be neglected to leading order in Ω. Hence, we let $\alpha = 1/2$ for a dominant balance and equation (2.8) simplifies to

$$\frac{\partial \delta \boldsymbol{x}}{\partial t} = D \frac{\partial^2 \delta \boldsymbol{x}}{\partial s^2} + J \delta \boldsymbol{x} + \boldsymbol{\eta} \,. \tag{2.9}$$

The reasoning behind choosing $\alpha = 1/2$ is analogous to the reasoning of the scaling in the weak noise expansion of van Kampen [33], especially the requirement that in the limit $\Omega \to \infty$ the noise correlations are zero. However, the system size in the external noise case is imposed by an external mechanism such as a non-modelled stochastic network with system size Ω.

The scaling of the perturbations to the steady state determines a hierarchy on the terms of equation (2.7) and in the case of non-inflow stochastic rate constants all multiplicative noise terms are linearised to additive terms with all non-trivial multiplicative perturbations only manifesting at higher order. The approach of this paper is similar to a weak noise approximation, however, with the fundamental difference that the weak noise expansion is used to approximate a probability distribution, whereas the perturbations to the steady state used in this paper approximate the local dynamics of a systems of PDEs.

Note, that equation (2.9) is mathematically equivalent to a chemical Langevin equation of compartmentalised diffusion in the limit of the compartment size, Δ_s, going to zero [36]. However, in our derivation the source of the noise is *external*. To emphasise the mathematical connection with internal noise we will in fact discretise equation (2.9) into a finite number of compartments, such that for an n species network

with $\mathcal{K}$ compartments we have

$$\delta\boldsymbol{x} = [\delta x_1, \dots, \delta x_{\mathcal{K}}, \delta x_{\mathcal{K}+1}, \dots, \delta x_{2\mathcal{K}}, \dots, \delta x_{n\mathcal{K}}]^T \,, \tag{2.10a}$$

$$\boldsymbol{\eta} = [\eta_1, \dots, \eta_{\mathcal{K}}, \eta_{\mathcal{K}+1}, \dots, \eta_{2\mathcal{K}}, \dots, \eta_{n\mathcal{K}}]^T \,, \tag{2.10b}$$

$$s \approx s_i = i\Delta_s \quad \text{where } i = \{1, \dots, \mathcal{K}\} \,, \tag{2.10c}$$

$$\frac{\partial^2 \delta\boldsymbol{x}(s)}{\partial s^2} \approx \frac{\delta\boldsymbol{x}(s_i + \Delta_s) + \delta\boldsymbol{x}(s_i - \Delta_s) - 2\delta\boldsymbol{x}(s_i)}{(\Delta_s)^2} \,, \tag{2.10d}$$

and the matrices D and J turn into block matrices such that

$$D = \begin{pmatrix} [D_1]_{\mathcal{K}\times\mathcal{K}} & 0 & 0 & \cdots \\ 0 & [D_2]_{\mathcal{K}\times\mathcal{K}} & 0 & \cdots \\ \vdots & \vdots & \vdots & \ddots \end{pmatrix} . \tag{2.11}$$

The ij^{th} block of J is $J_{ij} I_{\mathcal{K}\times\mathcal{K}}$ to give

$$J = \begin{pmatrix} [J_{11}]_{\mathcal{K}\times\mathcal{K}} & [J_{12}]_{\mathcal{K}\times\mathcal{K}} & \cdots \\ [J_{21}]_{\mathcal{K}\times\mathcal{K}} & [J_{22}]_{\mathcal{K}\times\mathcal{K}} & \cdots \\ [J_{31}]_{\mathcal{K}\times\mathcal{K}} & [J_{32}]_{\mathcal{K}\times\mathcal{K}} & \cdots \\ \vdots & \vdots & \ddots \end{pmatrix} . \tag{2.12}$$

Compartmentalisation results in a system of $n\mathcal{K}$ coupled SDEs

$$d\delta\boldsymbol{x} = A\delta\boldsymbol{x}\, dt + \boldsymbol{\eta}\, dt \,, \tag{2.13}$$

with $A = D/\Delta_s^2 + J$, $\langle \eta_i(t) \rangle = 0$ and $\langle \eta_i(t)\eta_j(t') \rangle = B_{ij} G_{ij}(t, t')$. Note that after compartmentalisation $B(s, s')$ is a block matrix of n^2 $\mathcal{K} \times \mathcal{K}$ matrices, describing the spatial auto-correlation of each species and the spatial correlations between species.

To calculate the power spectra of the system we introduce the discrete cosine transform [37]

$$f_\kappa = \Delta_s \sum_{j=1}^{\mathcal{K}} \cos[\kappa\Delta_s(j-1)] f(s_j) \,. \tag{2.14}$$

The cosine transform incorporates the von Neumann (no flux) boundary conditions, which are commonly used for reaction-diffusion systems, however, other boundary conditions can easily be implemented [37]. Due to the boundary conditions we require $\kappa = m\pi/l$ with $m \in \{0, 1, 2, \dots\}$. We refer to m as the *spatial mode*. Note that the use of $(j-1)$ instead of j which is due to the fact that the compartment labelling starts at $j = 1$. Hence, by applying the spatial Fourier transform we reduce the system of $n\mathcal{K}$ SDEs (2.13) to a system of n coupled SDEs

$$d\delta\boldsymbol{x}_\kappa = A_\kappa \delta\boldsymbol{x}_\kappa\, dt + \boldsymbol{\eta}_\kappa\, dt \,. \tag{2.15}$$

Finally, applying the temporal Fourier transform

$$\tilde{f}(\omega) = \int_{-\infty}^{\infty} f(t) e^{-i\omega t} dt \,, \tag{2.16}$$

we get an expression for $\delta\tilde{\boldsymbol{x}}_\kappa(\omega)$. Note that the Fourier transform always exists if we consider the system to have a fixed point [38].

$$\delta\tilde{\boldsymbol{x}}_\kappa(\omega) = [-A_\kappa - i\omega]^{-1} \tilde{\boldsymbol{\eta}}_\kappa(\omega) \,. \tag{2.17}$$

Therefore, the power spectra of the pattern, $P_{\delta x}(\kappa,\omega)$, can be expressed as the diagonal elements of

$$\langle \delta\tilde{\boldsymbol{x}}_\kappa(\omega)\delta\tilde{\boldsymbol{x}}_\kappa^\dagger(\omega)\rangle = \Phi^{-1}\underbrace{\langle\tilde{\boldsymbol{\eta}}_\kappa(\omega)\tilde{\boldsymbol{\eta}}_\kappa^\dagger(\omega)\rangle}_{N}\left(\Phi^{-1}\right)^\dagger\,, \tag{2.18}$$

where we defined

$$\Phi = -\left[A_\kappa + i\omega\right]\,, \tag{2.19}$$

and $\dagger$ denotes the hermitian conjugate of a matrix. In order to be guaranteed real power spectra we need $N = N^\dagger$. In the case of Gaussian noise we have

$$N = \mathcal{F}_{\cos}\left(\mathcal{F}(BG(t,t'))\right), \tag{2.20}$$

where $\mathcal{F}_{\cos}$ denotes the cosine transform and $\mathcal{F}$ the temporal Fourier transform. Note that when all temporal correlations are equal such that $G_{ij}(t,t') = g(t,t')$ the transform factor becomes

$$N = \mathcal{F}_{\cos}\left(B\right)\mathcal{F}(g(t,t')) = B_\kappa P_{\text{Correlations}}(\omega)\,, \tag{2.21}$$

where $P_{\text{Correlations}}$ is the power spectrum of the correlation function $g(t,t')$ and B_κ is the $n\times n$ matrix of covariances. For white noise we take $g(t,t') = \delta(t-t')/dt$ to reduce (2.13) to the Itô form

$$d\delta\boldsymbol{x} = A\delta\boldsymbol{x}\,dt + \boldsymbol{\eta}\,\sqrt{dt}\,, \tag{2.22}$$

with $\langle\eta_i(t)\eta_j(t')\rangle = B_{ij}\delta(t-t')$ and, therefore, $P_{\text{Correlations}} = 1$. Hence, we see that for white noise the power spectra are

$$\begin{aligned}\langle \delta\tilde{\boldsymbol{x}}_\kappa(\omega)\delta\tilde{\boldsymbol{x}}_\kappa^\dagger(\omega)\rangle &= \left[\Phi^{-1}\langle\tilde{\boldsymbol{\eta}}_\kappa(\omega)\tilde{\boldsymbol{\eta}}_\kappa^\dagger(\omega)\rangle\left(\Phi^{-1}\right)^\dagger\right] = \\ &= \left[\Phi^{-1}B_\kappa\left(\Phi^{-1}\right)^\dagger\right] = P_{\text{white}}\,.\end{aligned} \tag{2.23}$$

For general temporal correlations $g(t,t')$ we have

$$\begin{aligned}\langle \delta\tilde{\boldsymbol{x}}_\kappa(\omega)\delta\tilde{\boldsymbol{x}}_\kappa^\dagger(\omega)\rangle &= \left[\Phi^{-1}B_\kappa P_{\text{Correlations}}\left(\Phi^{-1}\right)^\dagger\right] = \\ &= P_{\text{white}}P_{\text{Correlations}}\,,\end{aligned} \tag{2.24}$$

such that the spectra of the noise colour appear as a multiplicative factor modulating the white noise spectra.

2.4. Application to the Schnakenberg System. We illustrate our analysis via the example of the Schnakenberg kinetics. The Schnakenberg system is an $n = 2$ species reaction-diffusion system which, despite its apparent simplicity, exhibits a wealth of different behaviours in the deterministic [39, 40, 41, 42] as well as stochastic [7, 35] regimes. The Schnakenberg system is a fully open system and, hence, both species can be subject to stochastic inflow. Hence, the Schnakenberg system is a perfect candidate to highlight the effects of coloured noise computationally and illustrate how the above analysis can be applied in practise. The system follows the reaction scheme

$$X_2 \xleftarrow{k_2} \emptyset \underset{k_{-1}}{\overset{k_1}{\rightleftharpoons}} X_1\,, \qquad\qquad 2X_1 + X_2 \xrightarrow{k_3} 3X_1\,. \tag{2.25}$$

The dynamics of the Schnakenberg system is described by the system of PDEs

$$\begin{aligned}\frac{\partial x_1}{\partial t} &= D_1\frac{\partial^2 x_1}{\partial s^2} + k_1 - k_{-1}x_1 + k_3 x_1^2 x_2,\\ \frac{\partial x_2}{\partial t} &= D_2\frac{\partial^2 x_2}{\partial s^2} + k_2 - k_3 x_1^2 x_2.\end{aligned} \tag{2.26}$$

First we check for a potential multistationarity in the Schnakenberg system by formulating the matrices m_1 and m_2.

$$m_1 = \begin{pmatrix} 1 & -1 & 0 & 1\\ 0 & 0 & 1 & -1\end{pmatrix} \qquad \text{and} \qquad m_2 = \begin{pmatrix} 0 & 0\\ 1 & 0\\ 0 & 0\\ 2 & 1\end{pmatrix}. \tag{2.27}$$

It is easy to check that $\ker(m_2) = \{0\}$. Further, we have

$$\sigma(\ker(m_1)) = \{(+,+,0,0)^T, (-,0,+,+)^T\}$$

and

$$\sigma(\mathrm{im}(m_2)) = \{(0,+,0,+)^T, (0,0,0,+)^T\}\,. \tag{2.28}$$

Hence, applying the injectivity criterion (2.4) we see that the Schnakenberg system is monostationary for all positive parameter values and, therefore, stochastic fluctuations in the inflow parameters cannot trigger stochastic switching.

Next, we consider stochastic inflows which result in $k_i \to k_i + 1/\sqrt{\Omega}\eta_i$ for $i \in \{1,2\}$ and the equations

$$\begin{aligned}\frac{\partial x_1}{\partial t} &= D_1\frac{\partial^2 x_1}{\partial s^2} + k_1 - k_{-1}x_1 + k_3 x_1^2 x_2 + \frac{1}{\sqrt{\Omega}}\eta_1,\\ \frac{\partial x_2}{\partial t} &= D_2\frac{\partial^2 x_2}{\partial s^2} + k_2 - k_3 x_1^2 x_2 + \frac{1}{\sqrt{\Omega}}\eta_2.\end{aligned} \tag{2.29}$$

Linearising equations (2.29) about the steady state $x_1^* = (k_1+k_2)k_{-1}^{-1}$, $x_2^* = k_2 k_{-1}^2 k_3^{-1}(k_1+k_2)^{-2}$ and discretising space we get a system of linear stochastic differential equations similar to the ones arising from the study of internal noise [7]

$$\frac{d\boldsymbol{x}}{dt} = A\boldsymbol{x} + \boldsymbol{\eta}, \tag{2.30}$$

with

$$A = \begin{pmatrix} \boldsymbol{a} & \boldsymbol{b}\\ \boldsymbol{c} & \boldsymbol{d}\end{pmatrix}, \tag{2.31}$$

where $\boldsymbol{a}, \boldsymbol{d}$ are tridiagonal matrices with diagonal elements

$$\begin{aligned} a_0 &= -2D_1/\Delta_s^2 - k_{-1} + 2k_3 x_1^* x_2^*,\\ d_0 &= -2D_2/\Delta_s^2 - k_3 x_1^{*2},\end{aligned} \tag{2.32}$$

and off-diagonal (sub- and super-diagonal) elements

$$\begin{aligned} a_1 &= D_1/\Delta_s^2 \equiv d_u,\\ d_1 &= D_2/\Delta_s^2 \equiv d_v.\end{aligned} \tag{2.33}$$

Colour	Correlation Function	Effect	Possible Origin	Section
White	1	N/A	internal	3.2
Ornstein-Uhlenbeck	$1/\left(\omega^2\tau^2+1\right)$	suppresses small ω	experimental apparatus	3.3
Red	$1/\omega^2$	excites small ω	deterministic	3.4
Predator-Prey	$\left(\alpha+\beta\omega^2\right)/\left(\omega^4+\gamma\omega^2+\delta\right)$	induces oscillations	stochastic subsystems	3.5

Table 1: An overview of our main results on various noise colours.

The matrices $\boldsymbol{b}$ and $\boldsymbol{c}$ are diagonal matrices with entries

$$\begin{aligned} b_0 &= k_3 x_1^{*2}, \\ c_0 &= -2k_3 x_1^* x_2^*. \end{aligned} \tag{2.34}$$

Note that the vector $\boldsymbol{x}$ has $2\mathcal{K}$ components. There are $\mathcal{K}$ components for species x_1 and $\mathcal{K}$ components for species x_2.

Hence, Fourier transforming equation (2.30) in space and time we can compute the power spectra,

$$P(\kappa,\omega) = \left[A_\kappa + i\omega\right]^{-1} \left\langle \tilde{\eta}_\kappa(\omega)\tilde{\eta}_\kappa^\dagger(\omega)\right\rangle \left(\left[A_\kappa + i\omega\right]^{-1}\right)^\dagger, \tag{2.35}$$

with

$$A_\kappa = \begin{pmatrix} a_0 + 2a_1\cos\kappa\Delta_s & b_0 \\ c_0 & d_0 + 2d_1\cos\kappa\Delta_s \end{pmatrix}. \tag{2.36}$$

In the following section we will discuss the effect of various noise correlations on the power spectra, and hence, the patterns generated.

3. Computational Results. In this section we highlight the computational patterns generated by a Turing system with coloured noise.

3.1. Numerical Methods. The system of SDEs (2.13) is simulated by an Euler-Maruyama scheme [43] with time step Δt such that

$$\boldsymbol{x}(t+\Delta t) = \boldsymbol{x}(t) + \boldsymbol{A}\boldsymbol{x}\Delta t + \boldsymbol{\eta}\Delta t. \tag{3.1}$$

The important step of the integration is to find the correct vector $\boldsymbol{\eta}$.

The white noise and Ornstein-Uhlenbeck noise are generated by an auxiliary noise process. In particular, at teach time step the white noise is sampled from a multivariate Gaussian distribution

$$\boldsymbol{\eta}\Delta t \sim \mathcal{N}(0, \boldsymbol{B}\Delta t).$$

The Ornstein-Uhlenbeck process is a generated by the stochastic differential equation

$$\frac{d\boldsymbol{\eta}}{dt} = -\frac{1}{\tau}\boldsymbol{\eta} + \frac{\sqrt{\boldsymbol{B}}}{\tau}\boldsymbol{\xi},$$

where $\boldsymbol{\xi}$ is a standard white noise vector. Therefore, at time t the vector $\boldsymbol{\eta}(t)$ is added to the to the system of SDEs. The Ornstein-Uhlenbeck "auxiliary equation" is integrated by an Euler-Maruyama scheme as described in [44].

To simulate power law noise for which, in general, no auxialiary SDE exists we use inverse transforms [45]. To generate a vector $\boldsymbol{\eta}(t)$ with correlations $\langle\boldsymbol{\eta}(t)\boldsymbol{\eta}^T(t')\rangle =$

$\boldsymbol{B}g(t-t')$, we first use the fact that $\boldsymbol{\eta} = \sqrt{\boldsymbol{B}}\boldsymbol{\xi}$ where $\boldsymbol{\xi}$ may be correlated in time but not in space, i.e. $\langle \boldsymbol{\xi}(t)\boldsymbol{\xi}^T(t')\rangle = \delta_{ij}g(t-t')$. Then, let the power spectrum of ξ_i be $1/\omega^\alpha$ as described in subsection 3.4 and use the algorithm of [45] to create a time series. Multiplication of $\boldsymbol{\xi}(t)$ with $\sqrt{\boldsymbol{B}}$ gives the desired noise process, $\boldsymbol{\eta}(t)$, which can be added to the SDE system. Auxiliary networks as in 3.5 can be simulated by either method and in this paper the auxiliary network input is generated by using the inverse transforms technique.

The truncation of the Gaussian distribution is implemented by setting negative values of the noise to zero at each time step. However, negative inflows were a rare occasion (for the simulation parameters chosen, only for violet noise any truncation was needed) and, hence, truncation had no effect on our simulations.

3.2. White Noise. First, we consider external white noise. In this special case the noise vector $\boldsymbol{\eta}$ is just a Wiener process with correlation matrix B. This case is mathematically identical to the case of internal noise in the weak noise limit as studied in [7]. The main differences between internal noise and the parameter noise considered in this paper are the amplitude of the noise and the exact forms of the covariances of the stochastic processes $\boldsymbol{\eta}$.

Both approximations (the weak noise limit, as well as our "truncated Gaussian" approximation) assume that the stochastic effect is a perturbation to the deterministic limit. However, as derived in [7], the covariance matrix of the stochastic processes $\boldsymbol{\eta}$ is determined by the microscopic processes whereas for external noise, whose origin can be manifold, the covariance matrix is arbitrary. For mathematical simplicity we choose the covariance matrix

$$B_\kappa = \begin{pmatrix} 1 & 1 \\ 1 & 1 \end{pmatrix}. \tag{3.2}$$

Throughout the remainder of this paper we fix the parameter values to

$$\begin{aligned} k_1 = k_2 = 10.0, \quad k_3 = 0.01, \quad k_{-1} = 20.0, \\ L = 0.1, \quad \mathcal{K} = 40, \end{aligned}$$

with diffusion coefficients

$$\begin{aligned} D_1 &= 10^{-4}, \\ D_2 &= 10^{-2}, \end{aligned} \tag{3.3}$$

which results in steady state concentrations of $x_1^* = 1$, $x_2^* = 1000$. The parameters chosen are not generic, but they represent a particularly interesting point in parameter space. The parameters are in the (stable) oscillatory regime of the Schnakenberg system and outside the Turing space. The main function of the noise will be to temporarily move the system into the Turing regime. Note that the system has large inflows (and outflows) compared to the chemical reaction parametrised by k_3 which allows for larger variations in the noise translating into larger pattern amplitudes. The modifications to the power spectra due to coloured noise are generic and apply all points in parameter space. However, the visibility of these modifications depends on the point in parameter space and the correlation matrix. Similarly, the results on amplitude of the patterns are parameter-dependent. To simulate the system, we discretise the space into 40 compartments of width $\Delta_s = 0.0025$ (which gives a total domain length of $L = 0.1$).

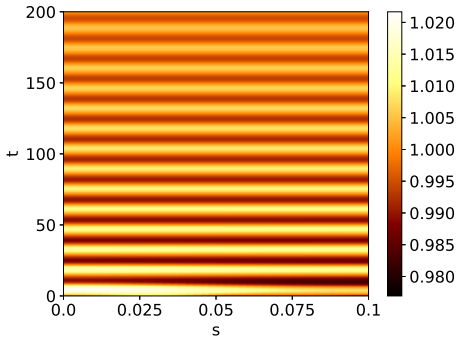

(a) The deterministic solution of the Turing system at the given parameter point

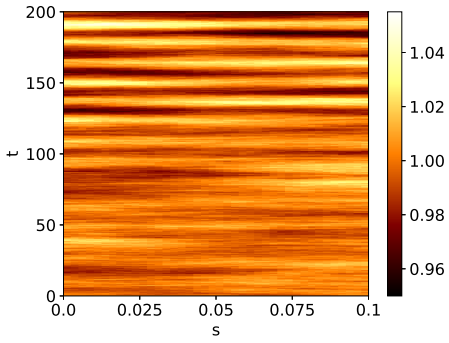

(b) A stochastic realisation with white noise

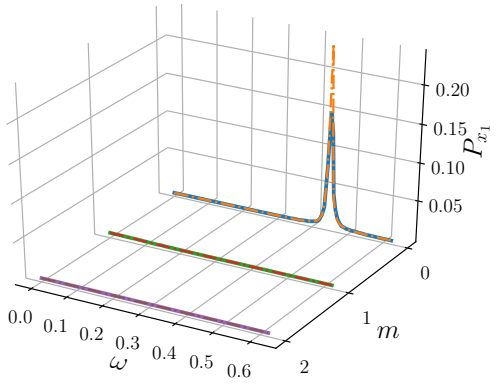

(c) The power spectra of the analytical calculations (dashed lines) and their simulated curves averaged over 50 realisations of length $T = 1000$ and subsystem size $\Omega = 5000$. We attribute the differences in peak height to the finite time steps used.

Fig. 2: An overview of the deterministic and white noise behaviour of the system with parameters as in (3.3). The peak in 2c at zero spatial mode, $m = 0$, indicates temporal oscillations which result from deterministic limit cycle oscillations. Due to the choice of reaction kinetics the temporal oscillations of species x_1 and x_2 are in phase.

Simulating equation (2.30) under the influence of white noise and with the given parameter values we obtain Figure 2 and its corresponding averaged power spectrum. The power spectrum shows the temporal frequencies, ω, and spatial modes, m, present in the pattern. The amplitude of the oscillations is about 3% of the steady state value for species x_1 whereas for species x_2 it is much lower. Therefore, we assume that any patterning of x_2 is not generally measurable and, therefore, we focus our attention

on x_1. The prominent temporal oscillations with no spatial dependency manifest themselves as a sharp peak in the power spectrum. This is due to the fact that the chosen parameter point is in the oscillatory regime of the Schnakenberg model. Upon close inspection slight spatial variations in the pattern of x_1 can be seen, but with white noise these are not very pronounced. In the following sections we show how noise colour can enhance spatial modes, create additional oscillations or even create a stable pattern.

3.3. Ornstein-Uhlenbeck Noise. Next, we investigate the effect of exponentially correlated noise also known as Ornstein-Uhlenbeck noise [46]. This stochastic process has a finite correlation time τ which we interpret as a response time. Consider an experiment in which the inflow rate is highly sensitive to the ambient temperature. Further, suppose this temperature undergoes random fluctuations about a regulated mean value. Therefore, the correlation time τ could represent the average response time of the temperature regulator.

We make the simplification that all the temporal correlations in equation (2.6) originate from Ornstein-Uhlenbeck processes with the same correlation time, τ, such that

$$g_{ij}(t,t') = g(t,t') = \frac{1}{2\tau} e^{-\frac{|t-t'|}{\tau}}. \tag{3.4}$$

Hence, it follows that

$$\langle \tilde{\eta}_\kappa(\omega) \tilde{\eta}_\kappa(\omega)^\dagger \rangle = B_\kappa \frac{1}{\omega^2\tau^2 + 1} \tag{3.5}$$

where B_κ is the same matrix as in the white noise case and therefore $P(\kappa,\omega)_{\text{Or-Uhl}} = P(\kappa,\omega)_{\text{white}}/(\omega^2\tau^2+1)$. Hence, the noise colouring will dampen temporal frequencies of $\omega \neq 0$ and, therefore, stabilise the pattern. Consequentially, in systems with Ornstein-Uhlenbeck noise we would expect any present stationary patterns that may be obscured by transient noise effects to be more prominent. We simulated the Schnakenberg system with Ornstein-Uhlenbeck noise and plotted the resulting patterns and power spectra in Figure 3. The pattern of x_2 has the same characteristic as in the white noise case, except for a smaller amplitude. Interestingly, x_1 shows a very different behaviour to the white noise case. Clear spatial structures can be seen, in particular the phenomenon of polarity switching [35, 7]. A Turing pattern of mode $m = 1$ is generated with a given polarity, namely, a minimum at $s = 0$ and a maximum at $s = L$ or vice versa. Polarity switching describes the inherently stochastic phenomenon of a sudden change in polarity as can be observed in Figure 3. The temporal oscillations, although still present, are reduced to a practically unobservable level. We attribute this to the fact that the exponential noise correlations dampen the oscillations present in the white noise system.

3.4. Power Law Noise. By power law noise we mean a stochastic process whose frequency distribution follows a power law in Fourier space

$$P_{\text{power}} = \frac{1}{\omega^\alpha}. \tag{3.6}$$

Various types of power law noise are common in engineering and are defined by colours summarised in Table 2. In this paper we study red noise, white noise (subsection 3.2) and violet noise to illustrate the effects of a positive, zero and negative exponent, α.

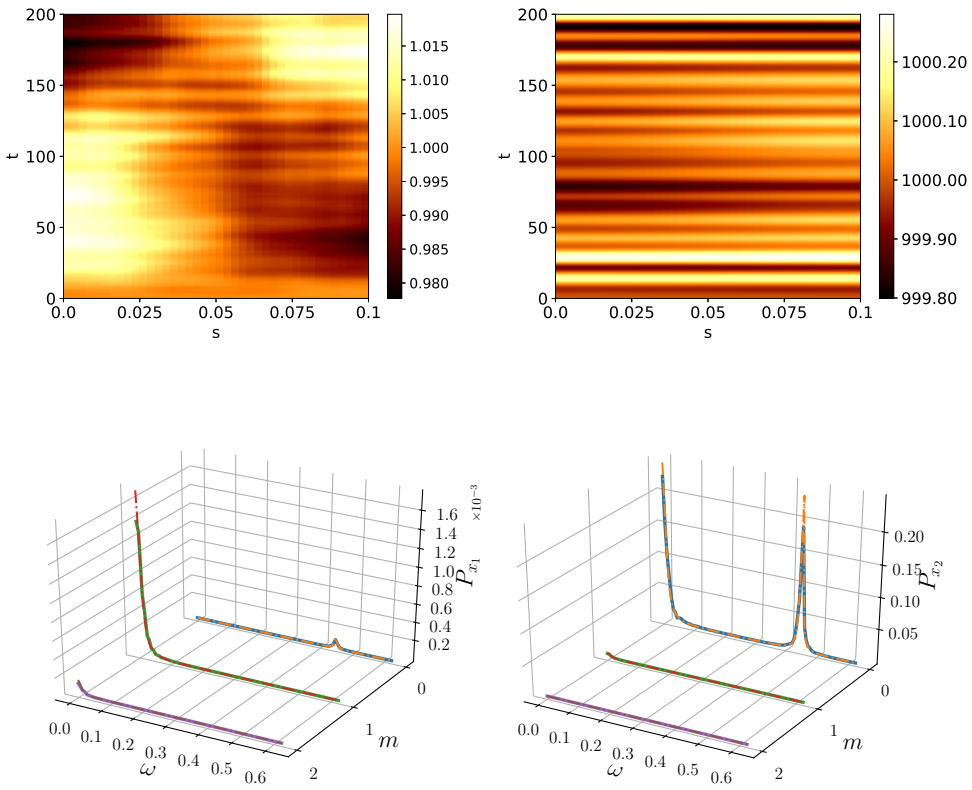

Fig. 3: The patterns and power spectra for the species x_1 (left) and x_2 (right) with noise generated by an Ornstein-Uhlenbeck process and $\tau = 100$. Spatial patterns become visible in the Ornstein-Uhlenbeck case which can be attributed to its dampening effect on temporal oscillations. This can be observed as a visible excitation of the $m = 1$ mode in the power spectrum of x_1 with the dashed line representing the analytical prediction. The well-known phenomenon of polarity switching [7] is observed in the pattern of x_1. The spectra were averaged over 50 repetitions with $T = 1000$ and subsystem size $\Omega = 100$.

Colour	α
Red	$\alpha = 2$
Pink	$\alpha = 1$
White	$\alpha = 0$
Blue	$\alpha = -1$
Violet	$\alpha = -2$

Table 2: The various colours of power law noise. In this paper we focus on red and violet noise.

Red noise amplifies small temporal frequencies with $1/\omega^2 \to \infty$ as $\omega \to 0$. Therefore, the zero frequency behaviour dominates the pattern. As can be seen in Figure 4, due to the amplification of small ω, the pattern becomes stable, even though the amplitude grows beyond the biologically viable (non-negative) bound indicating that non-linear effects need to be considered in the model. To investigate the red noise further, we look at the noise vector $\boldsymbol{\eta}$. For the simulation times chosen, $T = 1000$, the noise vector is independent of the time t such that each η_i has a constant, but random value. Hence, the effect of red noise is deterministic and equation (2.30) is just a linear ordinary differential equation with a constant drift term. After applying the spatial Fourier transform we obtain the equation

$$\frac{d\boldsymbol{\delta x}_\kappa}{dt} = A_\kappa \boldsymbol{\delta x}_\kappa + \boldsymbol{\eta}_\kappa, \tag{3.7}$$

and denoting the eigenvalues and eigenvectors of A_κ as $\lambda_1(\kappa)$, $\lambda_2(\kappa)$ and $\boldsymbol{\nu}_1(\kappa)$, $\boldsymbol{\nu}_2(\kappa)$ respectively, the linear equation can be solved to give

$$\boldsymbol{\delta x}_\kappa(t) = c_1 \boldsymbol{\nu}_1(\kappa) e^{\lambda_1(\kappa)t} + c_2 \boldsymbol{\nu}_2(\kappa) e^{\lambda_2(\kappa)t} - A_\kappa^{-1} \boldsymbol{\eta}_\kappa, \tag{3.8}$$

where c_1 and c_2 are constants determined by the initial conditions. Investigating the spatial mode $m = 0$, which corresponds to the dynamics of the non-spatial system, we find that the dynamics corresponds to a stable spiral and, therefore, transient oscillations around $\omega \approx 0.5$ are expected. Indeed, it can be seen in Figure 4 that transient oscillations are present and in order to calculate the power spectrum accurately only the time points in $t \in [800, 1000]$ are used. If the entire data were used for the calculation of power spectra a peak at $\omega \approx 0.5$ would appear which is not accounted for in the analytic spectrum. The same caveat does not apply to other coloured noise processes due to the constantly varying perturbations to the steady state.

To illustrate the behaviour of the system on the other end of the colour spectrum, and to highlight the limits of our analysis, we simulated violet noise which stabilised the temporal oscillations further and due to large power at large ω drove the oscillation amplitude in the linear treatment to unphysical values. Again, this indicates that violet noise cannot be treated in biological applications with a simple linear theory, but a full non-linear theory must be used. For violet noise the effect of the truncation of the Gaussian became too large to obtain an accurate prediction of the power spectra as can be seen in Figure 5. Further, while noise colours with positive exponent are actively studied in biology [47], the potential emergence of blue or violet noise in applications is not clear.

3.5. Stochastic Auxiliary Networks. We now proceed to the second major source of random inflows, namely the dependence on a stochastic auxiliary network. An auxiliary network is a chemical reaction network which provides an input into the Turing system (see Figure 6). The auxiliary network is connected to the main network only via an inflow reaction and, if the auxiliary network reaches a steady state, it can be subsumed into the zero complex for practical modelling. If, however, the auxiliary network exhibits more complex dynamics such as deterministic or stochastic oscillations, then it needs to be treated as a part of the main network. We focus on auxiliary networks which are deterministically stable, but show stochastic quasi-cycles. The dynamics of such systems are modelled by using a correlated stochastic inflow parameter as outlined in section 2.2.

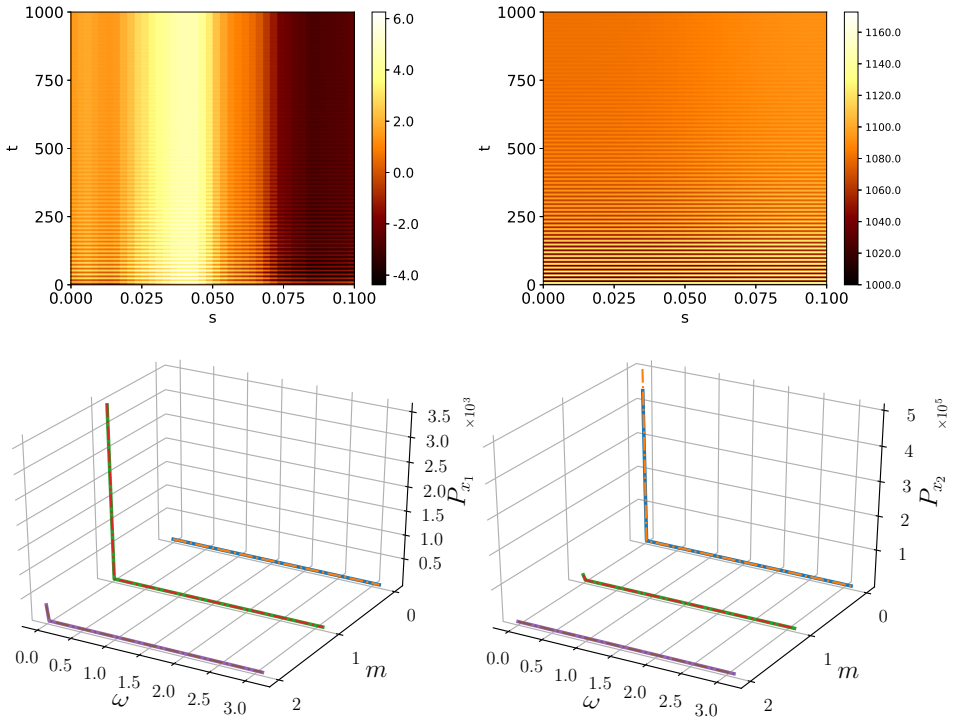

Fig. 4: The patterns and power spectra for the species x_1 (left) and x_2 (right) with noise generated by a red noise process. As predicted, the spectra are dominated by the behaviour the $\omega = 0$, which amounts to the stabilisation of a particular spatial mode. The species concentrations, however, go negative indicating that a full non-linear model needs to be used. The peak in the power spectrum for x_2 is a numerical artefact. The spectra were averaged over 50 repetitions with simulation time $T = 200$. The subsystem size was $\Omega = 5000$.

As an illustrative example we use the predator-prey system described in [8],

$$\begin{aligned} Y_1 &\xrightarrow{d_1} \emptyset \xleftarrow{d_2} Y_2, \\ 2Y_1 &\xleftarrow{p_1} Y_1 + Y_2 \xrightarrow{p_2} Y_1. \end{aligned} \tag{3.9}$$

In [8] it was shown that in the deterministic regime the system (3.9) has exactly one attractor for any choice of rate constants. Hence, as the inflow parameters k_1 and k_2 are proportional to the concentration of Y_1, they will have a constant value. However, when the copy numbers of Y_1 and Y_2 are small and stochastic fluctuations are important the predator-prey model (3.9) can exhibit so-called "quasi-cycles" which are stochastic analogue of limit-cycles and manifest themselves as peaks in the power spectra.

Consider this "predator-prey noise" in a Schnakenberg system. Suppose the inflows k_1 and k_2 in the Schnakenberg system depend on the presence of the chemical species Y_1, such that $k_1 \propto y_1$ and $k_2 \propto y_1$, where y_1 denotes the concentration of Y_1.

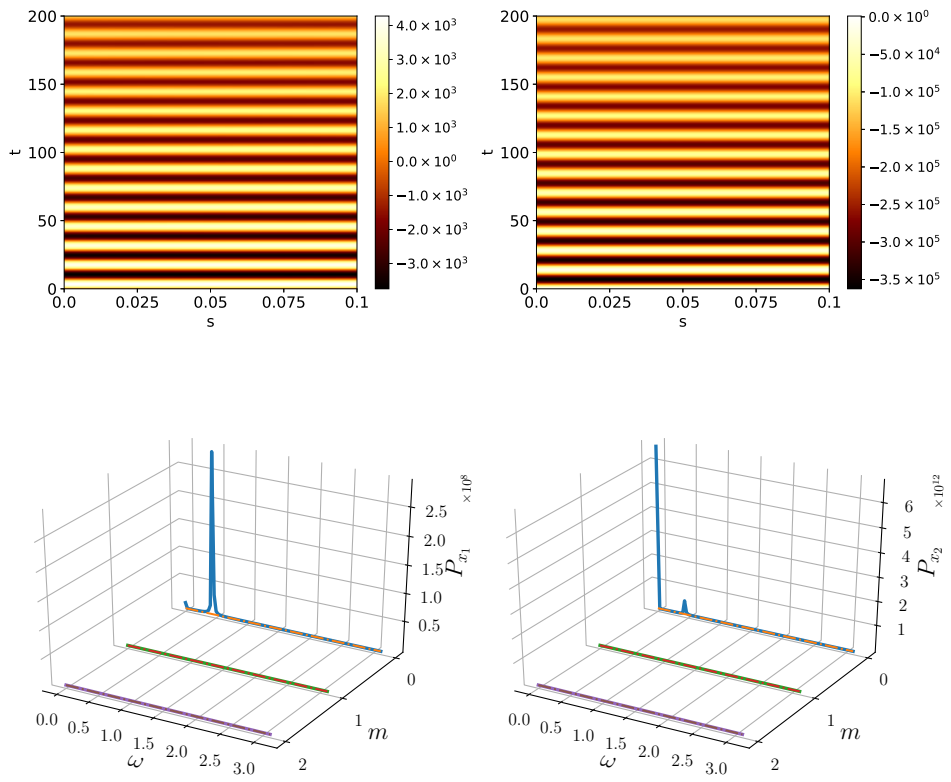

Fig. 5: The patterns and power spectra for x_1 (left) and x_2 (right) with noise generated by a violet noise process. The discrepancy in the power spectra originates from the truncation of the Gaussian process. The negative species concentrations indicate that a non-linear theory needs to be used to fully model a violet noise system. The spectra were averaged over 50 repetitions with simulation time $T = 200$. The subsystem size was $\Omega = 5000$.

Again, we assume $g_{ij}(t, t') = g(t, t')$ for mathematical simplification. In Fourier space the power spectrum of Y_1 is

$$P_{\text{Predator-Prey}} = \frac{\alpha + \beta\omega^2}{(\omega^2 + \Omega_0^2) + \Gamma^2\omega^2}, \tag{3.10}$$

where we use the parameter values from [8] $\alpha = 0.000384$, $\beta = \Gamma = 0.04$, $\Omega_0^2 = 0.016$.

Equation (3.10) has a peak at $\omega \sim 0.06$, so we expect peaks at a similar frequency for each non-zero spatial mode in the power spectrum of the Schnakenberg system. The resulting patterns and the corresponding average power spectra are presented in Figure 7. The power spectra gained a second peak in the $m = 0$ mode and peak in all modes $m > 0$ at $\omega \sim 0.06$. Therefore, it can be seen that a deterministic parent system can inherit the dynamics of a stochastic auxiliary network and mix it with its own intrinsic dynamics.

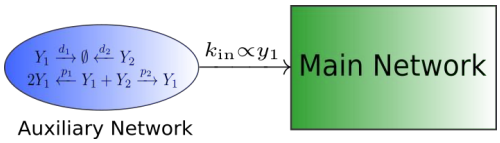

Fig. 6: A schematic of an auxiliary network and its input to the main system. This is a specific example of scenario (b) of Figure 1.

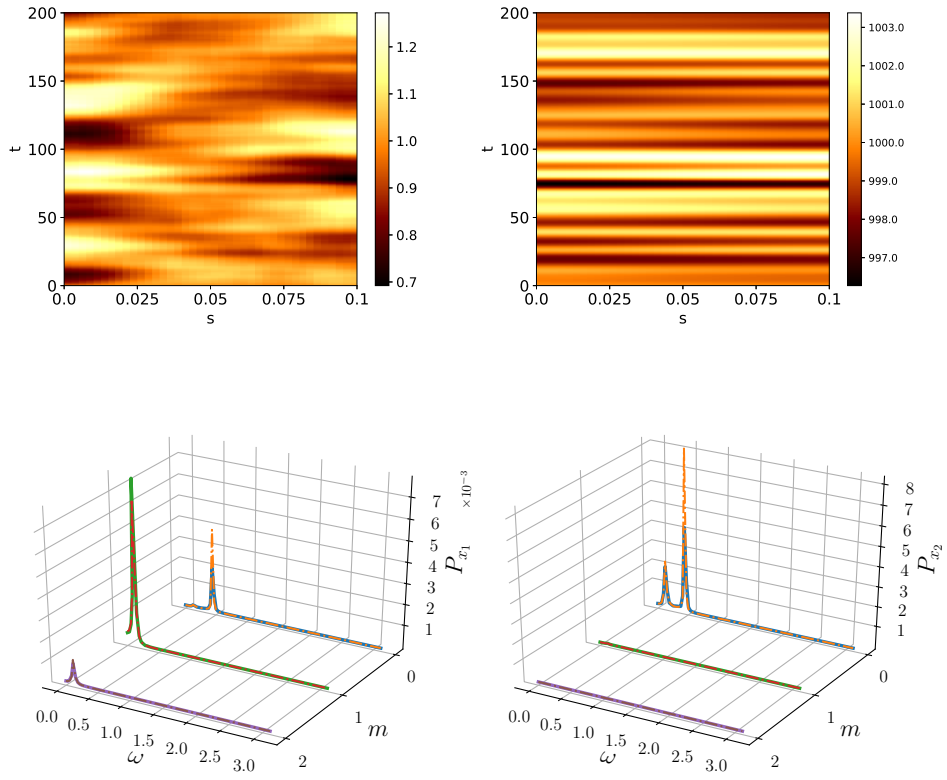

Fig. 7: The power spectra for the species x_1 (left) and x_2 (right) with noise generated by a stochastic predator-prey network [8]. The power spectra inherited a second peak from the subsystem which activates oscillatory modes on top of the deterministic oscillation frequency. The spectra were averaged over 50 repetitions and simulation time $T = 200$ with m indexing the spatial mode. The subsystem size was $\Omega = 100$.

3.6. Mixed Noise. Next, we investigated the case of mixing noise processes, in particular, we consider an Ornstein-Uhlenbeck process which has a different correlation time for x_1 and x_2, τ_1 and τ_2 respectively. Then we let $\tau_2 \to 0$ in order to recover the white noise case for species two.

We introduce the auxiliary normal stochastic processes ξ and hence, the spatial

modes of the noise η_κ are described by [46]

$$\frac{d\eta_\kappa}{dt} = -\begin{pmatrix} \frac{1}{\tau_1} & 0 \\ 0 & \frac{1}{\tau_2} \end{pmatrix} \eta_\kappa + \begin{pmatrix} \frac{1}{\tau_1} & 0 \\ 0 & \frac{1}{\tau_2} \end{pmatrix} b_\kappa \xi, \tag{3.11}$$

where b_κ is a 2×4 matrix satisfying $b_\kappa b_\kappa^T = B_\kappa$. We Fourier transform (3.11) and define the matrix,

$$\phi = \begin{pmatrix} \frac{1}{\tau_1} + i\omega & 0 \\ 0 & \frac{1}{\tau_2} + i\omega \end{pmatrix} \tag{3.12}$$

to give

$$\tilde{\eta}_\kappa = \phi^{-1} \begin{pmatrix} \frac{1}{\tau_1} & 0 \\ 0 & \frac{1}{\tau_2} \end{pmatrix} b_\kappa \tilde{\xi}. \tag{3.13}$$

Letting $\tau_2 \to 0$ and computing the covariance matrix gives

$$N = \langle \tilde{\eta}_\kappa(\omega) \tilde{\eta}_\kappa(\omega)^\dagger \rangle = \begin{pmatrix} B_{\kappa,11} \frac{1}{1+\omega^2\tau_1^2} & B_{\kappa,12} \frac{1}{1+i\omega\tau_1} \\ B_{\kappa,12} \frac{1}{1-i\omega\tau_1} & B_{\kappa,22} \end{pmatrix}, \tag{3.14}$$

where $B_{k,ij}$ are the ij^{th} elements of the B_κ matrix. Note that N is hermitian and therefore we expect real power spectra for the patterns of x_1 and x_2.

Simulating equation (2.9) with the noise process described by (3.11) gives rise to the mixed patterns seen in Figure 8. Note, that computationally the limit $\tau_2 \to 0$ is equal to setting τ_2 to the time step dt. The patterns of both species appear similar to the pure Ornstein-Uhlenbeck patterns, however, with reduced amplitude.

3.7. Reduced Stochastic Inflows. In the final subsection we instigate the case of only species x_1 being subjected to stochastic inflows. The species x_2 is assumed to only have deterministic inflow at a rate k_2 and $\eta_2 = 0$. Hence, the correlation matrices N will be reduced to

$$N = \begin{pmatrix} \langle \tilde{\eta}_{1\kappa} \tilde{\eta}_{1\kappa}^* \rangle & 0 \\ 0 & 0 \end{pmatrix}. \tag{3.15}$$

In the noise processes studied in this paper the behaviour of the species is virtually unchanged and the patterning is robust with respect to disregarding cross-correlations.

4. Conclusion. In this paper we investigated the effect of stochastic inflows on a deterministic reaction-diffusion system. We restricted the class of networks considered to monostationary systems and used results from real algebraic geometry to show how monostationarity is related to network structure. We then introduced a stochastic perturbation to an inflow reaction as a truncated Gaussian process with the expectation value at the deterministic inflow parameter. After linearising we computed the power spectra for arbitrary noise colours and showed that in simple cases the power spectra can be derived as a multiplicative factor. The remainder of the paper consisted of applying our analysis to the Schnakenberg system and highlighting the effects various noise colouring can have on a reaction-diffusion system.

We briefly restated the results from the white noise analysis, proceeding to add coloured noise and then demonstrating its effect by computing the power spectra. In particular, for the simple case when all species experience the same temporal correlations, the power spectra of the correlations appear as a multiplicative factor in

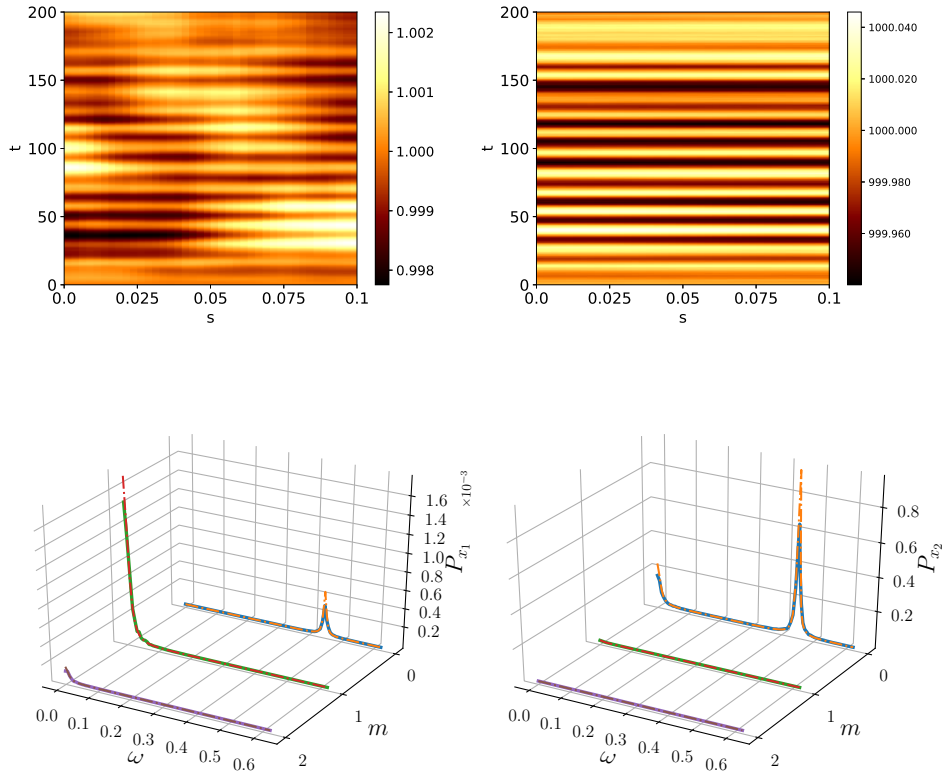

Fig. 8: The patterns generated for the species x_1 (left) and x_2 (right) with Ornstein-Uhlenbeck noise and $\tau = 100$ for x_1 and x_2 with white noise.The patterns are phenomenologically similar to the Ornstein-Uhlenbeck patterns, however, with reduced amplitude. The power spectrum of x_2 is a mixture of white noise and Ornstein-Uhlenbeck noise. The power spectra were averaged over 50 simulations with simulation time $T = 1000$ and subsystem size $\Omega = 5000$.

the total power spectra. Hence, depending on the nature of the correlations they will suppress or excite temporal frequencies at all spatial modes. Ornstein-Uhlenbeck noise has a Lorentzian frequency distribution and, therefore, suppresses positive frequencies. Power law noise can either completely stabilise or destabilise the pattern depending on the sign of the exponent, α. This is due to the fact that for positive α temporal frequencies at $\omega = 0$ go to infinity and, therefore, all oscillations are suppressed which results in a stable pattern which resembles a pattern arising from simulations inside the Turing regime.

For the simulation times used in this paper, the noise vector was actually constant, and, therefore, deterministic methods could be used to study the stabilising effect of pink or red noise. The opposite is the case for negative α where the frequency contribution in the power spectrum increases as ω increases and oscillations are enhanced. However, certain aspects of the red, blue, or violet, noise cases cannot be explained by

our simple analytic prediction. The significance and the correct analytic description of blue/violet noise could form a part of further work.

When turning to stochastic auxiliary networks we see that the reaction-diffusion system can inherit traits of the dynamics of the auxiliary network. In particular, we showed that when the auxiliary network exhibits a predator-prey dynamic with stochastic oscillations these oscillations can still be observed in the deterministic main network. We concluded the range of applications by considering mixed noise with Ornstein-Uhlenbeck input for species x_1 and white noise for species x_2. In this case, the system behaves similar to a system with pure Ornstein-Uhlenbeck dynamics and differences can only be found by a power spectral analysis. Finally, we observed in the cases considered that when only one species experiences stochastic inflow the patterns created are, except for potential special cases, similar to the ones when the inflow to both species is randomised. However, the extent to which such results may hold in generality is for further work.

Further directions could also include attempting to relate these studies to potential mechanisms of left-right symmetry breaking amplification in developmental biology, in particular the impact of induced Nodal production on one side of the embryonic node, which is hypothesised to be driven by ciliary fluid flows and also highly error-prone [48]. It is generally asserted that the resulting interactions of the gene products Nodal and Lefty, which are major contenders as Turing morphogens [49, 50, 51], amplify this initial error-prone signal to generate robust patterning, driving downstream developmental left-right asymmetry. However, the ability of Turing systems to amplify the spatially localised, error-prone, and thus stochastic, influx of activator morphogen [48, Figure 2] to robustly amplify a stochastic symmetry breaking in self-organisation, as well as any additional constraints required to do so, is theoretically untested. Thus examining the mechanistic basis of these postulates in this critical developmental biological process provides a fundamental application for the theoretical foundations developed here.

REFERENCES

[1] J. D. Murray. *Mathematical Biology II - Spatial Models and Biomedical Applications*, volume 18 of *Interdisciplinary Applied Mathematics*. Springer-Verlag, New York, 3 edition, 2008.

[2] D. Hochberg, F. Lesmes, F. Morán, and J. Pérez-Mercader. Large-scale emergent properties of an autocatalytic reaction-diffusion model subject to noise. *Phys. Rev. E*, 68(6), 2003.

[3] A. Turing. The chemical basis of morphogenesis. *Philos. Trans. R. Soc. London B Biol. Sci.*, 237(641):37–72, 1952.

[4] A. J. McKane, T. Biancalani, and T. Rogers. Stochastic pattern formation and spontaneous polarisation: the linear noise approximation and beyond. *Bull. Math. Biol.*, 76(4):895–921, 2014.

[5] T. Butler and N. Goldenfeld. Robust ecological pattern formation induced by demographic noise. *Phys. Rev. E*, 84:011112, 2011.

[6] D. Xavier. *On the theory of cell migration: durotaxis and chemotaxis*. PhD thesis, Universitat Politcnica de Catalunya, 2013.

[7] L. J. Schumacher, T. E. Woolley, and R. E. Baker. Noise-induced temporal dynamics in turing systems. *Phys. Rev. E*, 87(4):042719, 2013.

[8] A. J. McKane and T. J. Newman. Predator-prey cycles from resonant amplification of demographic stochasticity. *Phys. Rev. Lett.*, 94(21):218102, 2005.

[9] T. Biancalani, T. Galla, and A. J. McKane. Stochastic waves in a brusselator model with nonlocal interaction. *Phys. Rev. E*, 84:026201, 2011.

[10] T. E. Woolley, R. E. Baker, E. A. Gaffney, P. K. Maini, and S. Seirin-Lee. Effects of intrinsic stochasticity on delayed reaction-diffusion patterning systems. *Phys. Rev. E*, 85(5):051914, 2012.

[11] T. E. Woolley, R. E. Baker, E. A. Gaffney, and P. K. Maini. Influence of stochastic domain

growth on pattern nucleation for diffusive systems with internal noise. *Phys. Rev. E*, 84(4):041905, 2011.

[12] J. García-Ojalvo and J. Sancho. *Noise in Spatially Extended Systems*. Springer Science & Business Media, 2012.

[13] D. T. Gillespie. The chemical Langevin equation. *Jour. Chem. Phys.*, 113(1):297–306, 2000.

[14] T. Dauxois, F. Di Patti, D. Fanelli, and A. J. McKane. Enhanced stochastic oscillations in autocatalytic reactions. *Phys. Rev. E*, 79(3):036112, 2009.

[15] F. Sagués, J. M. Sancho, and J. García-Ojalvo. Spatiotemporal order out of noise. *Rev. Mod. Phys.*, 79(3):829, 2007.

[16] D. T. Gillespie. Exact stochastic simulation of coupled chemical reactions. *Jour. Phys. Chem.*, 81(25):2340–2361, 1977.

[17] B. Alberts, A. Johnson, J. Lewis, M. Raff, K. Roberts, and P. Walter. *Molecular Biology of the Cell*. Garland Science, 2007.

[18] F. Horn and R. Jackson. General mass action kinetics. *Arch. Rat. Mech. and Anal.*, 47(2):81–116, 1972.

[19] T. E. Woolley, R. E. Baker, and P. K. Maini. Turing's theory of morphogenesis: where we started, where we are and where we want to go. In *The Incomputable*, pages 219–235. Springer, 2017.

[20] S. Müller, E. Feliu, G. Regensburger, C. Conradi, A. Shiu, and A. Dickenstein. Sign conditions for injectivity of generalized polynomial maps with applications to chemical reaction networks and real algebraic geometry. *Found. Comput. Math.*, 16(1):69–97, 2016.

[21] V. Castets, E. Dulos, J. Boissonade, and P. De Kepper. Experimental evidence of a sustained standing turing-type nonequilibrium chemical pattern. *Phys. Rev. Lett.*, 64:2953–2956, 1990.

[22] J. H. E. Cartwright. Labyrinthine turing pattern formation in the cerebral cortex. *Jour. Theo. Biol.*, 217(1):97 – 103, 2002.

[23] Sh. Kondo and T. Miura. Reaction-diffusion model as a framework for understanding biological pattern formation. *Science*, 329(5999):1616–1620, 2010.

[24] N. Picco, E. Sahai, P. K. Maini, and A. R. A. Anderson. Integrating models to quantify environment mediated drug resistance. *Cancer Research*, 77(19):5409–5418, 2017.

[25] O. Lenive, P. D. W. Kirk, and M. P. H. Stumpf. Inferring extrinsic noise from single-cell gene expression data using approximate bayesian computation. *BMC Syst. Biol.*, 10(1):81, aug 2016.

[26] M. Feinberg. Chemical reaction network structure and the stability of complex isothermal reactors-I. the deficiency zero and deficiency one theorems. *Chem. Eng. Sci.*, 42(10):2229–2268, 1987.

[27] M. Feinberg. Chemical reaction network structure and the stability of complex isothermal reactors-II. multiple steady states for networks of deficiency one. *Chem. Eng. Sci.*, 43(1):1–25, 1988.

[28] K. Banerjee and K. Bhattacharyya. Open chemical reaction networks, steady-state loads and braess-like paradox. *ArXiv e-prints*, 2014.

[29] B. Joshi and A. Shiu. A survey of methods for deciding whether a reaction network is multistationary. *ArXiv e-prints*, 2014.

[30] B. Félix, A. Shiu, and Z. Woodstock. Analyzing multistationarity in chemical reaction networks using the determinant optimization method. *Appl. Math. Comput.*, 287-288:60–73, 2016.

[31] M. Banaji and C. Pantea. The inheritance of nondegenerate multistationarity in chemical reaction networks. *SIAM Jour. Appl. Math.*, 78(2):1105–1130, 2018.

[32] S. A. Frank. Input-output relations in biological systems: measurement, information and the hill equation. *Biol. Direct*, 8:31, 2013.

[33] N. G. van Kampen. *Stochastic Processes in Physics and Chemistry*. Elsevier, 1983.

[34] M. F. Adamer, T. E. Woolley, and H. A. Harrington. Graph-facilitated resonant mode counting in stochastic interaction networks. *Jour. Roy. Soc. Interface*, 14(137), 2017.

[35] T. E. Woolley, R. E. Baker, E. A. Gaffney, and P. K. Maini. Stochastic reaction and diffusion on growing domains: Understanding the breakdown of robust pattern formation. *Phys. Rev. E*, 84(4):046216, 2011.

[36] G. D. Smith. *Numerical solution of partial differential equations, Finite difference methods*. Clarendon Press, 1985.

[37] W. Briggs and V. Henson. *The DFT: An Owner's Manual for the Discrete Fourier Transform*. Society for Industrial and Applied Mathematics, 1995.

[38] T. E. Woolley, R. E. Baker, E. A. Gaffney, and P. K. Maini. Power spectra methods for a stochastic description of diffusion on deterministically growing domains. *Phys. Rev. E*, 84(8718):21915, 2011.

[39] D. Iron, J. Wei, and M. Winter. Stability analysis of turing patterns generated by the schnakenberg model. *J. Math. Biol.*, 49(4):358–390, 2004.

[40] P. K. Maini, T. E. Woolley, R. E. Baker, E. A. Gaffney, and S. S. Lee. Turing's model for biological pattern formation and the robustness problem. *J. Roy. Soc. Interface Focus*, 2(4):487–496, 2012.

[41] M. J. Ward and J. Wei. The existence and stability of asymmetric spike patterns for the schnakenberg model. *Stud. Appl. Math.*, 109(3):229–264, 2002.

[42] E. H. Flach, S. Schnell, and J. Norbury. Turing pattern outside of the turing domain. *Appl. Math. Lett.*, 20(9):959–963, 2007.

[43] Peter E. Kloeden and Eckhard. Platen. *Numerical solution of stochastic differential equations*. Springer-Verlag, 1995.

[44] G N Milshtein and M V Tret 'yakov. Numerical solution of differential equations with colored noise. *J. Stat. Phys.*, 774(3), 1994.

[45] J. Timmer and M. Koenig. On generating power law noise. *Astronomay and Astrophysics*, 300:707, 1995.

[46] P. Hanggi and P. Jung. Colored noise in dynamical systems. *Adv. Chem. Physics. Vol LXXXIX*, LXXXIX:239–326, 1995.

[47] P. Szendro, G. Vincze, and A. Szasz. Bio-response to white noise excitation. *Electro- and Magnetobiology*, 20(2):215–229, 2001.

[48] M. Blum, K. Feistel, T. Thumberger, and A. Schweickert. The evolution and conservation of left-right patterning mechanisms. *Development*, 141(8):1603–1613, 2014.

[49] P. Müller, K. W. Rogers, B. M. Jordan, J. S. Lee, D. Robson, S. Ramanathan, and A. F. Schier. Differential diffusivity of nodal and lefty underlies a reaction-diffusion patterning system. *Science*, 336(6082):721–724, 2012.

[50] Y. Chen and A. F. Schier. Lefty proteins are long-range inhibitors of squint-mediated nodal signaling. *Curr. Biol.*, 12(24):2124–2128, 2002.

[51] A. F. Schier. Nodal signaling in vertebrate development. *Annu. Rev. Cell Dev. Biol.*, 19(1):589–621, 2003.